Journal of Materials Chemistry C

Porosity induced rigidochromism in platinum(II) terpyridyl luminophores immobilized at silica composites

Journal:	*Journal of Materials Chemistry C*
Manuscript ID	TC-ART-02-2021-000599.R1
Article Type:	Paper
Date Submitted by the Author:	11-Apr-2021
Complete List of Authors:	Norton, Amie; USDA Agricultural Research Service, Grain Quality and Structure Zanoni, Kassio; Universidad de Valencia, Instituto de Ciencia Molecular Dourges, Marie-Anne; Universite de Bordeaux College Sciences et Technologies Ravaro, Leandro; Universidade de São Paulo Abdolmaleki, Mahmood; Unversity of Cincinnati, Dept. of Chemistry de Camargo, Andrea; Institut of Physics of Sao Carlos, University of Sao Paulo, Applied Phyisics; Universitaet Muenster, Institut fuer Physikalische Chemie Toupance, Thierry; University of Bordeaux, Institut des Sciences Moléculaires, UMR 5255 CNRS, 351 Cours de la Libération Connick, William; University of Cincinnati, Chemistry Chatterjee, Sayandev; Pacific Northwest National Laboratory, Energy and Environment Directorate

Porosity induced rigidochromism in platinum(II) terpyridyl luminophores immobilized at silica composites

Amie E. Norton [1,2,*] Kassio P. S. Zanoni [3,4], Marie-Anne Dourges [5], Leandro P. Ravaro [3], Mahmood K. Abdolmaleki [1,6], Andrea S. S. de Camargo [3], Thierry Toupance [5], William B. Connick [1,a], and Sayandev Chatterjee [7,*]

1. Department of Chemistry, University of Cincinnati, Cincinnati, OH 45220.
2. Present Address: USDA-ARS Grain Quality and Structure, 1515 College Ave. Manhattan, KS 66503; *Email: amie.norton@usda.gov.*
3. Laboratório de Espectroscopia de Materiais Funcionais (LEMAF), Instituto de Física de São Carlos, Universidade de São Paulo, 13566-590, São Carlos – SP, Brazil.
4. Present Address: Molecular Opto-Electronic Devices (MOED), Instituto de Ciencia Molecular, Parque Cientifico, Universidad de Valencia, 46980 Paterna, Spain.
5. Univ. Bordeaux, Institute of Molecular Chemistry, UMR 5255 CNRS, 351 Cours de la Libération, F-33405 Talence Cédex, France.
6. Present Address: Department of Biology and Chemistry, Texas A&M International University, Laredo, TX, 78041, USA.
7. ESSENCE Diagnostics LLC, Livingston, NJ 07039; *Email: sayandev@essencediagnostics.com*
a. *In memoriam of Dr. William B. Connick who passed away May 18, 2018.*

ABSTRACT

Stimuli responsive composites consisting of inorganic or organometallic coordination substrates supported on porous platforms that integrate and improve the key features of both the substrate and platform, open the doorway to advanced multifunctional materials. This work presents a new class of stimuli responsive multifunctional materials based on platinum(II) terpyridyl luminophores@silica composites. Presented herein is the impact of intercalation of Pt(II) salts with a planar architecture and sterically permitting terpyridyl ligands within meso or microporous silica support, on their spectroscopies. The photophysics and luminescence properties of square-planar Pt(II) salts are governed by their intermolecular, non-covalent Pt•••Pt interactions between the individual Pt(II) units; a feature that has been explored in designing stimuli responsive materials. This work explores a novel methodology where the electronic structure and luminescence behavior of such salts are systematically varied through their intercalation within rigid silica frameworks. The intercalation of Pt(II) complexes with varied degrees of non-covalent Pt•••Pt interactions in the virgin form within meso-macroporous silica supports generates materials that show marked variation in their electronic structure and luminescence behavior compared to their virgin salts. Further, the spectroscopies show a systematic dependance on the mean pore size of the silica support. The X-ray powder diffraction and microscopy studies reveal these behaviors to be related to the

perturbations in their long-range structural order, that gets reflected in their microcrystalline dimensions and particle morphologies.

KEY WORDS

stimuli responsive composites; hybrid materials; smart materials; luminescent sensors; inorganic frameworks; mesoporous composites

INTRODUCTION

Composite hybrid materials consisting of functional inorganic or organometallic substrates supported on porous platforms have received growing consideration as they open the doorway to the design of new advanced multifunctional materials.[1] The integration of metal complexes with porous, high surface area frameworks, for example, leads to hybrid materials of significance due to their evolved structural design, the added functions they provide at the support interface, and structural robustness and enhanced sensitivity by the virtue of their meso- or microporous crystalline environment.[1-9] In recent years, researchers have incorporated luminescent *d*-block complexes in a range of support materials (prominent ones being silica or polymer based supports) for sensing[10], imaging[11], drug delivery[12] and catalytic applications.[13] These studies demonstrate the ability of the transition metal complexes to being incorporated within pores of diameters as small as 3-6 nm.[14-15]

In terms of sensing applications, particularly attractive is the intercalation of stimuli responsive transition metal complexes whose luminescence properties can be altered by external perturbations such as variations in temperature, pressure, exposure to anions or vapor molecules. Among the various possible *d*-block metal complexes, coordinatively-unsaturated square-planar Pt(II) complexes exhibit intriguing spectroscopic properties that can be orchestrated by controlling the non-covalent interactions through their vacant axial sites.[16-24] This general tendency has been utilized in designing Pt(II) salts with a planar architecture and sterically permitting ligands, where the variations in color and luminescence are governed by their intermolecular, non-covalent Pt•••Pt interactions between the individual Pt(II) units.[25-41] These interactions can be modified by external stimuli such as mechanical or thermal force or exposure to an external solvent or vapor guest, which induces structural reorganization to alter the Pt•••Pt spacings and result in prominent changes in their photophysics. This finds applications in the design of stimuli-responsive mechanochromic, thermochromic, solvatochromic or vapochromic luminescent materials.[26, 42-50] Furthermore, incorporation of such Pt(II) centers into porous or engineered material supports can generate new hybrid materials with diverse and expanded applications, while also allowing practical robustness, operational flexibility, and reproducibility. This has been demonstrated through the application of silica or polymer platform supported Pt(II) complexes for studies of vapor/gas response,[43, 51-56] temperature/pressure sensing,[57] drug delivery,[58] protein binding,[59] catalysis,[60-62] imaging,[63] photosensitization,[14-15, 38, 64-65] and oxygen sensing.[66-67] Thus, Pt(II) complexes have been covalently attached to mesoporous supports (*e.g.*, sol gels, ion exchange resins, MCM-41, SBA-15) in studies of vapochromism[68] and $^1O_2$ sensitization.[14, 38, 64-65] However, the mentioned examples represent discrete independent studies; consequently a systematic understanding of how pore size of the porous framework affects the Pt•••Pt interactions, and impacts the ultimate photophysics of the Pt(II)@composite hybrids is lacking, limiting the selection of the support materials for sensing applications. Of particular interest would be scenarios where the complexes can be tailored to exhibit a pronounced shift of their luminescence bands that is dictated by the rigidity of their matrix; a tendency that is termed as "luminescence rigidochromism".[69]

This work investigates the impact of systematic variations in pore size of the porous support platforms on the ultimate photophysics of the Pt(II)@composites. Among the various available support materials, macro- (pore diameter > 50 nm), meso- (2 < pore diameter < 50 nm) and microporous (pore diameter < 2 nm) silica-based supports are widely used because of their high surface area, appreciable thermal stability, high stability under acidic conditions, simple preparation and scale up, and ability to be easily functionalized.[70] Silica based porous materials allow for the encapsulation of functional molecules within the pores while also enabling the diffusion of various guest species (solvents, gases or ions) into the material, making them conducive to sensing applications.[66] Furthermore, these materials also allow systematic variation of the pore sizes. Taking advantage of this last property, this work focuses on probing the photophysical properties of representative square-planar Pt(II) salts when supported on controlled pore glass (CPGs) type meso or macroporous silica and the impact of systematic variations in the pore sizes on their absorption and emission properties.

It can be anticipated that the pore sizes and structure of the porous platform can influence the photophysics of coordinatively unsaturated Pt(II) salts by dictating their packing in two complementary ways; (i) by either restricting the dispersion of individual Pt(II) units in an oriented way that is better suited for stronger Pt•••Pt interactions compared to their randomized arrangement in powder form yielding a bathochromic shift in luminescence, or (ii) conversely restraining aggregation of the individual Pt(II) units and restricting the Pt•••Pt interactions to result in a hypsochromic shift. To probe these possibilities, two different Pt(II) salts are chosen. The first chosen Pt(II) complex, namely $[Pt(tpy)Cl]PF_6$ (**1**●PF_6; tpy = 2,2′;6′,2″-terpyridine; **Figure 1** (left)) is characterized by comparatively weak non-covalent Pt•••Pt interactions in the parent form. The crystal structure of the parent form consists of the individual $[Pt(tpy)Cl]^+$ units grouped as distinct dimers, with the interdimer distances being considerably long.[71-73] However, the presence of a sterically permitting tpy ligand with complementary σ-donating and π-accepting character and the availability of open axial sites on each dimeric unit permits the dimers to approach each other for more elaborate Pt•••Pt non-covalent, intermolecular interactions upon the application of the appropriate external stimuli. This tendency has been demonstrated by the salt upon its exposure to MeCN vapors or solvents,[72] or during the substitution of the PF_6^- anion with ClO_4^-,[73] which led to structural reorganization leading to the shortening of the Pt•••Pt interactions. The other Pt(II) complex chosen for this study is $[Pt(tpy)Cl]ClO_4$●H_2O (**1**●ClO_4●H_2O; **Figure 1** (center)), which shows extensive and strong Pt•••Pt non-covalent interactions in the parent crystal structure.[73-74] The axial sites of the individual [Pt(tpy)Cl] units in this salt are already engaged in short interactions with the neighboring Pt(II) units; therefore the structure cannot permit further shortening of Pt•••Pt to further strengthen these interactions. On the contrary, it is possible to disrupt the extensive Pt•••Pt non-covalent interactions through the application of specific external perturbations, as it has been demonstrated by thermal activation of **1**●ClO_4●H_2O that led to loss of the solvate water molecule, and resulted in structural reorganization of the **1**●ClO_4 structure, with weakened Pt•••Pt interactions.[73-74] Therefore, these two systems complement each other in presenting two extreme scenarios; one where the Pt•••Pt non-covalent interactions are present in a limited capacity in the parent form as in **1**●PF_6 but can be readily extended; the other where such interactions are present extensively in the parent state which can be disrupted as in **1**●ClO_4●H_2O. This work investigates how the incorporation of these salts within a porous framework alters the photophysics of these complexes. Furthermore, this work also probes how the variation in CPG pore sizes from 70-1599 Å impacts the Pt•••Pt interactions, and consequently their photophysical properties. It is anticipated that when the species are incorporated within a porous environment, the pore size and volume will also have a potential impact on the Pt•••Pt stacking interactions. Further, in order to compare and contrast the effect of the various pore sizes on the ability of the transition metal complex to partake in M•••M interactions, the spectroscopic properties of the two platinum(II) salts@silica composite are compared and contrasted with a compound that is sterically

restricted from participating in intermolecular M•••M interactions, namely an octahedral Ru(II) salt, $[Ru(bpy)_3]Cl_2$ (**2**●Cl_2, bpy = 2,2′-bipyridine; **Figure 1** (right)), with well documented spectroscopic and luminescent properties.[75] **2**●Cl_2 has a rigid coordination environment whose structure cannot accommodate M•••M interactions upon external perturbations, and therefore acts as a control system.

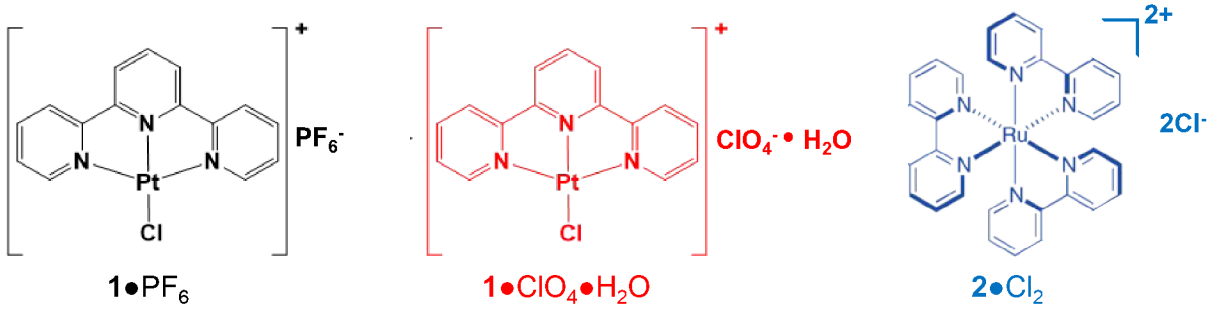

Figure 1. Molecular structures of the three complexes investigated in this work: $[Pt(tpy)Cl]PF_6$ (**1**●PF_6; left), $[Pt(tpy)Cl]ClO_4$●H_2O (**1**●ClO_4●H_2O; center), $[Ru(bpy)_3]Cl_2$ (**2**●Cl_2; right).

RESULTS AND DISCUSSIONS

Spectroscopic characterization of 1●PF_6@silica.

The effect of association of the yellow **1**●PF_6 salt onto different silica substrates was probed visually as well as using spectroscopic techniques. Unless mentioned otherwise, DMSO/acetone was used for **1**●PF_6 loading. This was dictated by the complete solubility of the salt in DMSO/acetone, which would lead to more efficient loading. Further, this solvent mixture does not affect the chemical integrity of the salt as verified by NMR and mass spectrometry studies (mass spectra shown in ESI **Figure S1**). The various silica supports used were CPGs of seven different sizes (70 Å, 383 Å, 537 Å, 623 Å, 815 Å,1057 Å and 1599 Å) as well as non-porous silica (NP-SiO_2) and MCM-41 (21 Å pore size), which were each loaded with equal amounts of **1**●PF_6 (0.005:0.1 g/g **1**●PF_6: silica) as described in the Experimental Section.

Association of the yellow **1**●PF_6 salt with different porous silica substrates results in a distinct coloration of the substrates. It is observed that the color tones depend on the pore sizes, with the smaller pore CPGs (70 Å, 383 Å and 537 Å), MCM-41 and NP-SiO_2 demonstrating progressive bathochromic shifts compared to the larger pore CPGs (**Figure 2**), ascribed to an increasing stabilization of the lowest-lying ^{3}MMLCT transition associated with a [dσ*(Pt)→ π*(tpy)] transition. The dσ* arises from the platinum d_z^2 orbital-interactions of adjacent $[Pt(tpy)Cl]^+$ units.[73-74, 76] An enhancement in the intermolecular Pt•••Pt interactions as the pore environment gets more restricted with the shrinking of the CPG pore sizes, leads to increased energies of the dσ*.[77] The changes in the contact solution colors are shown in ESI **Figure S2**. Further, a visual inspection of the loaded materials under UV irradiation shows that for the **1**●PF_6@CPGs, the color of emission progressively changes from reddish-orange to orange and finally to yellow as the pore sizes increased, **Figure 2.** In fact, the **1**●PF_6@MCM-41 materials having the smallest pore size of 21 Å shows an intense orangish-red emission under UV light.

As summarized earlier, the **1**●PF_6 salt itself either as powder or in crystal form shows comparatively weak Pt•••Pt interactions, as indicated by its crystal structure.[72] The parent crystal structure shows $[Pt(tpy)Cl]^+$ units grouped as distinct dimers with alternate short and long intermolecular Pt•••Pt distances, the intradimer and interdimer distances being 3.3502(3) and 4.0315(3) Å units respectively. However, the accessibility of the open axial sites and the presence of a ligand with strong σ-donating and π-accepting

character such as 2,2′:6′,2″-terpyridine[76] make the system conducive to accommodate more extensive and stronger Pt•••Pt interactions under appropriate circumstances. This is possible in instances where there is an adequate steric and/or electronic drive to accommodate such a change. One possible method is through the incorporation of guest chemical species with the right steric and electronic complementarity within the structural framework, which can lead to a structural rearrangement that alters the stacking of the individual $[Pt(tpy)Cl]^+$ units and therefore the Pt•••Pt interactions. The electronic structure of these complexes being strongly dependent on the Pt•••Pt interactions, this results in a simultaneous change in their optical properties.[78-79] This has been widely explored in the chemical sensing capabilities of the **1**●PF_6 salt, in the form of vapors (e.g. MeCN,)[72] solvents (e.g. MeCN),[29] or anions (e.g. ClO_4^-,).[73] In these instances, the steric drive was provided by the structural rearrangement in the host Pt(II) lattice due to the incorporation of the guest vapor, solvent or anion. The visible observations of the bathochromic shift in color and luminescence spectroscopies in the **1**●PF_6 salt upon its loading onto/into the silica support indicate a similar rearrangement leading to closer approach of the Pt(II) units. This points to the likelihood of the rigid silica framework prompting stronger Pt•••Pt interactions compared to the randomized arrangement of the Pt(II) units in powder form.

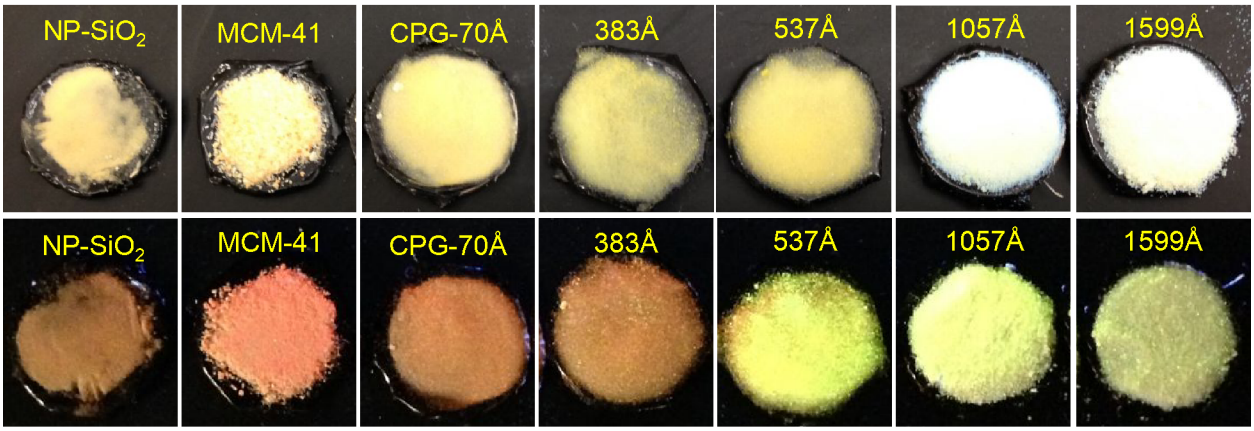

Figure 2. Photographs of **1**●PF_6 loaded onto silica supports: (top panels) Observed under UV light (λ_{ex}=365 nm) and (bottom panles) under ambient light.

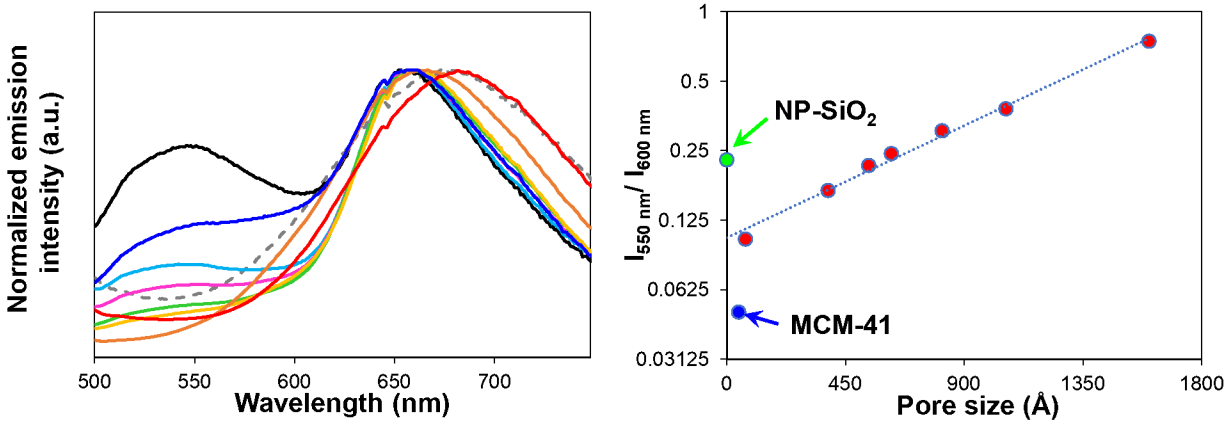

Figure 3. (left panel) Normalized emission spectra of **1**●PF_6@silica composites (λ_{ex}=436 nm): (——) CPG-1599 Å, (——) CPG-1057 Å, (——) CPG-815 Å, (——) CPG-623 Å, (——) CPG-537 Å, (——) CPG-383 Å, (——) CPG-70 Å, (——) MCM-41, (----) NP-SiO_2. (right panel) A semi-logarithmic dependence of the intensity ratios of the ~550 nm and the ~650 nm bands on the pore size of the silica

support. (Red circles) CPGs, (green circle) NP-SiO_2, (blue circle) MCM-41. The equation of the line for the CPGs: $\log(I_{550\ nm}/I_{630\ nm}) = 0.0005\times$pore size – 0.9825.

Table 1. Summary of emission maxima of various **1**●PF_6 and **1**●PF_6@silica substrates

Material	Emission Band Maxima (nm)	
	Higher energy band	Lower energy band
1●PF_6@NP SiO_2	np	676
1●PF_6@MCM-41	np	685
1●PF_6@CPG-70Å	546 (sh)	670
1●PF_6@CPG-383Å	546 (sh)	663
1●PF_6@CPG-537Å	546 (sh)	661
1●PF_6@CPG-623Å	547	660
1●PF_6@CPG-815Å	549	657
1●PF_6@CPG-1057Å	550	656
1●PF_6@CPG-1599Å	550	650
1●PF_6 Crystals	np	550
1●PF_6 Powder*	550 (sh)	650 (br)
1●PF_6 deposited on glass slide from DMSO: acetone	550	680
1●PF_6 deposited on glass slide from water: acetone	np	550

np = not present; sh = shoulder; br = broad. *emission is from reference 29

Emission spectroscopy was conducted to quantitatively probe the changes in the electronic structure of the salt upon its association with the silica support. Their emission spectra are exhibited in **Figure 3** and the emission features of the various substrates upon excitation at 436 nm are listed in **Table 1**. The comparative emsision spectra of **1**●PF_6@silica composites relative to pristine **1**●PF_6 in shown in ESI **Figure S3**. For measuring the emission, the **1**●PF_6@silica composites were layered on a microscopic glass slide as described in the Experimental Section, and the emission profiles were recorded upon excitation at λ_{exc} = 436 nm.

It is observed that the **1**●PF_6@CPG composite with the largest studied pore size, namely 1599 Å, shows two features, one centered at 650 nm and a second feature with lower intensity near ~550 nm. The feature near 550 nm is assigned to ^{3}LC/MLCT mixed states,[76, 80-81] based on its similarity with a ~550 nm emission band observed in crystals or microcrystalline samples of **1**●PF_6.[76] On the other hand, the 650 nm band is assigned to the lowest-lying ^{3}MMLCT excited state. This band has been reported to be extensively influenced by non-covalent, intermolecular Pt•••Pt interactions, *vide infra*.[76, 78] This band has also been shown to be highly sensitive to sample preparation, as noted by the differences in emission energies between microcrystals in this work and powders reported by Bailey and coworkers.[78] In this work, the relative intensity of the band near 550 nm is observed to progressively decrease relative to the 650 nm band intensity as the pore size decreased, to the extent that the 550 nm band is relegated to a shoulder and is nearly non-existent for the CPGs with pore sizes ranging from 0-537Å. This intensity enhancement of the 630 nm band relative to the 550 nm band with decreasing the pore size suggests that the non-covalent, Pt•••Pt interactions are exclusively highlighted with decreasing pore size. Simultaneously, the ^{3}MMLCT band centered at 650 nm for **1**●PF_6@CPG-1599 Å is observed to gradually shift to higher wavelengths as the mean pore size decreases, as summarized in **Table 1**.

In fact, a careful examination of the relative emission intensities of the ~550 nm and the ~650 nm band shows an intriguing correlation with the pore size of the silica support. It is observed that the semi-logarithm

of the intensity ratios of the ~550 nm to the ~650 nm band for the various **1**●PF_6@CPGs increases proportionally with the pore size (**Figure 3, right panel**). The same emission profiles were observed for the **1**●PF_6@CPGs at other excitations, as reflected in the emission profiles observed upon excitation of select **1**●PF_6@CPGs at wavelengths of 365, 410, and 436 nm respectively, as shown in **ESI Figure S4**. These emissions are also observed to show the same dependence of the ~550 nm to the ~650 nm bands with the pore size of the silica support. Therefore, there is a direct dependence of the spectroscopies of the **1**●PF_6@silica composites and their Pt•••Pt interactions on the mean pore size of the silica support. A comparison of the emission spectroscopy of **1**●PF_6@silica with pure **1**●PF_6 powders demonstrates greater similarities of the **1**●PF_6@silica materials with larger pore sizes with **1**●PF_6 powders. For example, the **1**●PF_6 powders have been reported to show an extremely broad emission at room temperature centered at ~650 nm, with a shoulder at ~550 nm.[78] It is worth noting that the **1**●PF_6@MCM-41 and **1**●PF_6@NP-SiO_2 emissions deviate from the linear trend as shown in **Figure 3, right panel.** This suggests the photophysics for these two composites might be of different nature than the **1**●PF_6@CPGs.

These observations of (i) the linear dependance of the emission profiles of the **1**●PF_6@silica hybrids with the pore size of the silica support, and (ii) spectral similarity of the **1**●PF_6@large pore silica with **1**●PF_6 powders, cumulatively point to **1**●PF_6 intercalation within the silica pores. If such an intercalation was absent, the likelihood of a systematic correlation of the spectral intensity of the ^{3}MMLCT transition with the pore size would be unlikely or serendipitous. Furthermore, it is likely that the larger pores allow more freedom for the platinum units to randomize and orient themselves in various possible ways that may be comparable to the unsupported powder material. In the smaller pore sizes, the units are more restrained which forces them to aggregate in a directed way which becomes effective in highlighting the Pt•••Pt interactions. This rigidochromic effect is also responsible for the shift in the emission wavelength with pore size. It is worth pointing that the deviation of the **1**●PF_6@MCM-41 and **1**●PF_6@NP-SiO_2 emission spectroscopies from the linear trend demonstrated by the **1**●PF_6@CPGs is presumably suggestive of a different kind of association of the Pt(II) salt with these materials.

Additionally, excitation spectra were recorded on selected **1**●PF_6@silica composites at the λ_{max} of the emissive features assigned to the ^{3}LC/MLCT and ^{3}MMLCT states, namely at 550 nm and 630 nm. The excitation spectra are all characterized by a band at ~368 nm that has been tentatively assigned to ^{1}MLCT and a second feature ~448 nm that is associated with the ^{1}MMLCT absorption,[76] and features at higher wavelengths. The ~448 nm band exhibits a significant dependence on Pt•••Pt interactions, as reported[76] and corroborated by our results.

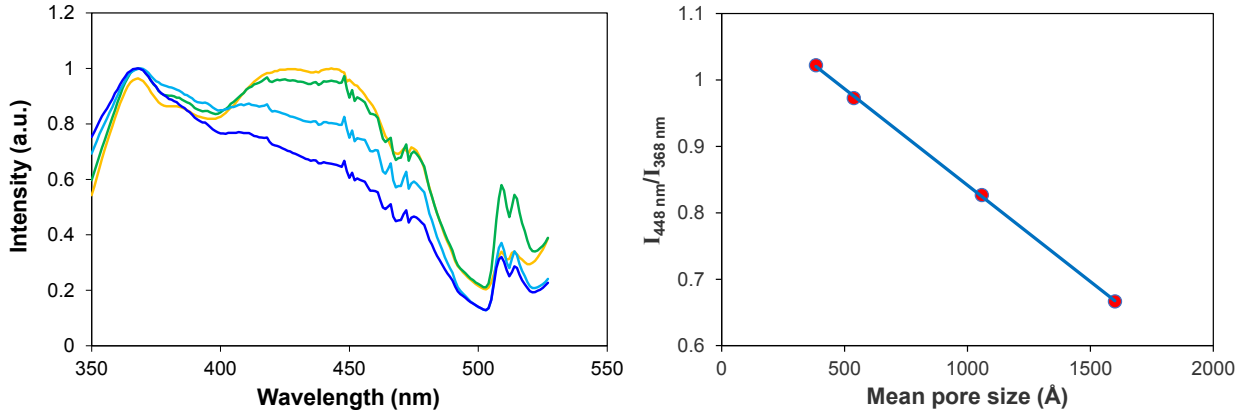

Figure 4. (left panel) Normalized excitation spectra of **1**●PF_6@silica composites monitored at λ_{em} = 550 nm: (—) CPG-1599 Å, (—) CPG-1057 Å, (—) CPG-537 Å, (—) CPG-383 Å. (right panel) Ratio of the excitation bands at 448/368 vs pore size. The equation of the line: $I_{448\ nm}/I_{368\ nm}$ = -0.0003×pore size + 1.1316.

The intensity ratios of the ~448 nm excitation band to the ~368 nm excitation band ($I_{448\ nm}/I_{368\ nm}$) progressively decreases with increasing of the mean pore size. In a behavior that is complementary to the dependence of emission intensities with pore sizes of the silica supports, the intensity ratios of the ~448 nm to the ~360 nm band for the various **1**●PF_6@CPGs shows an inverse linear relationship with the pore size (**Figure 4**). A similar behavior is observed in the excitation spectra of the **1**●PF_6@CPGs for the 630 nm emission band as shown in ESI **Figure S5**.

The effects of various loading parameters on the luminescent behavior of the **1**●PF_6@CPGs were also investigated. The CPGs were loaded with the **1**●PF_6 three times in succession (0.005:0.1 w/w × 3), and emissions were recorded after each loading. With each consecutive loading, the intensity of the ^{3}LC/MLCT band at lower wavelength increased compared to the ^{3}MMLCT band at longer wavelength for the CPGs (ESI **Figure S6**). This was reflected in the increase in the emission intensity of the lower wavelngth shoulders for the **1**●PF_6@CPGs with CPG pore sizes of 383 and 537 Å, while for 1057 Å a new band was observed to appear at ~550 nm. This selective increase in the relative intensity of the higher energy ^{3}LC/MLCT relative to the lower energy ^{3}MMLCT is supportive of intercalation of the materials within the pores. If surface deposition was the only mode of association between the platinum salt and the CPGs, such deposition would have increased the overall Pt aggregation and therefore increase the intensity of both the ^{3}LC/MLCT and ^{3}MMLCT. The fact that the intensity of the ^{3}LC/MLCT band increases at a higher rate compared to the ^{3}MMLCT suggests that the pores might get saturated with higher platinum loading, and subsequently the salt gets deposited on the surface, at which point the material tends to behave more like unrestricted powdered **1**●PF_6 salt.

Additionally, the emission was observed to be unaffected by drying times (4 hours vs 24 hours; ESI **Figure S7**) and variable excitation wavelengths (365, 410, 436 nm; as discussed earlier and shown in ESI **Figure S4**). The loading solvent however was observed to play a significant role (ESI **Figure S8**). Two solvent systems were used to demonstrate the solvent effects, namely (1:1 DMSO:acetone mixture and 1:1 water:acetone mixture). It is worth noting the complex was insoluble or sparingly soluble in most solvents. Therefore, DMSO was chosen as the primary solubilizing solvent it allows an appreciable solubility for the salt over a range of salt concentrations. Acetone was chosen as the secondary solvent due to its strong interaction with silica, that facilitates the interaction of the Pt(II) salts with the silica. Among the other solvents tried, the complex showed sparing solubility. Therefore, as an experimental control, water was chosen as a solvent to examine the impact of using a loading solvent where the solubility of the salt is highly limited, and probe its impact on the spectroscopy.

In water:acetone, the low energy band at ~550 nm predominates in all the CPGs with the exception of the 383 Å, while the lower energy band at ~660 nm is relegated to almost a shoulder. This is presumably due to the higher solubility of the **1**●PF_6 salt in the former solvent set compared to the latter. In the water:acetone solution, it is possible that contact with the CPGs induces inhomogeneous precipitation of the **1**●PF_6 units on the surface, and the emission behavior partly resembles the microcrystalline **1**●PF_6 samples. Finally, the **1**●PF_6@CPGs were observed to be fairly robust with time, as no prominent changes were observed in their emission characteristics of intensities over time (ESI **Figure S9**).

It is worth pointing that the composite formed in the association of the Pt(II) salt with the non-porous silica support, namely **1**●PF_6@NP-SiO_2, shows among the most effective red luminescence. This indicates that

surface association with the silica framework of the support plays a key role in dictating the photophysics of the **1**●PF_6 salt. However, the variation and systematic trends in the ^{3}MMLCT transitions across the range of **1**●PF_6@silica materials where the porosity of the silica is the only variable, indicates that this variation is induced by the silica porosity, and therefore points to an intercalation of the salt into the silica. In the absence of any intercalation, the only form of association will be the surface interaction of the Pt(II) salt with the silica. Such surface interaction is unlikely to systematically vary across a range of silica-based materials depending upon the porosity. It should be noted that while a plot of the ^{3}MMLCT energies of the **1**●PF_6@CPGs show a linear correlation with their porosity, the **1**●PF_6@NP-SiO_2 and **1**●PF_6@MCM-41 composites deviate from this linearity, suggesting a different association for these two materials. Therefore, the porosity dependent linear variation in **1**●PF_6@CPG emission energies point to their intercalation within the silica pores, while the deviation of the **1**●PF_6@NP-SiO_2 and **1**●PF_6@MCM-41 from this dependance is presumably due to a surface association. It is also to be pointed out that in all the silica materials including the CPGs, surface deposition does take place as it is unlikely for the entire Pt(II) salt to get intercalated within the CPGs.

The systematic variation of the photophysics and emission energies of the **1**●PF_6@CPGs with the pore size of the CPGs opens the possibilities of the applicability of similar rigidochromic composites to determine the pore size of silicas by using a fast, easy, and economic technique. It is worth mentioning that measurements of the emission maximum have a standard error of ±1 nm, which is comparable to the differences in the energy maximum of the lowest energy ^{3}MMLCT transition for several of the **1**●PF_6@CPGs as shown in **Table 1**. Therefore, relying on the absolute changes in the energy of this band for estimating the pore size of the CPGs would be unreliable. However, there is a distinct variation in the relative intensity changes of the lowest energy ^{3}MMLCT and the higher energy ^{3}LC/MLCT band located at ~550 nm, and the variation of this ratio with the CPG pore size gives a more accurate and reliable estimation of the pore size. It is to be noted that this work provides only a proof-of-concept validation of the qualitative applicability of this method in assessing the pore sizes of silica-based frameworks. Our future studies will be invested in more focused probing of the sensibility of this and similar square-planar composites to establish a certain pore size.[82-84] This proof-of-the-concept demonstration also provides a potential method for a fast, economic assessment of the porosities of other engineered porous frameworks as well.

Spectroscopic characterization of 1●ClO_4●H_2O@silica

The observation of the enhancement of Pt•••Pt interactions in the **1**●PF_6 salt upon its intercalation in the porous silica framework motivated us to examine an analogous system where the extensive, non-covalent Pt•••Pt interactions are already preexistent in the parent form.[85] **1**●ClO_4●H_2O is an example of such a species where non-covalent Pt•••Pt interactions are already present to the fullest extent in the parent form. The crystals of this complex already demonstrate strong and extensive Pt•••Pt interactions showing a nearly linear chain (Pt•••Pt•••Pt=166.81(2)°) with short Pt•••Pt distances (3.3031(5), 3.3692(5) Å). The emission spectra of this salt in powder form, upon excitation at 436 nm, shows a broad band centered at 700 nm **(Figure 5(A))**, ascribed to the lowest-lying ^{3}MMLCT ($d\sigma^*(Pt) \rightarrow \pi^*(tpy)$) transition.[73-74, 78]

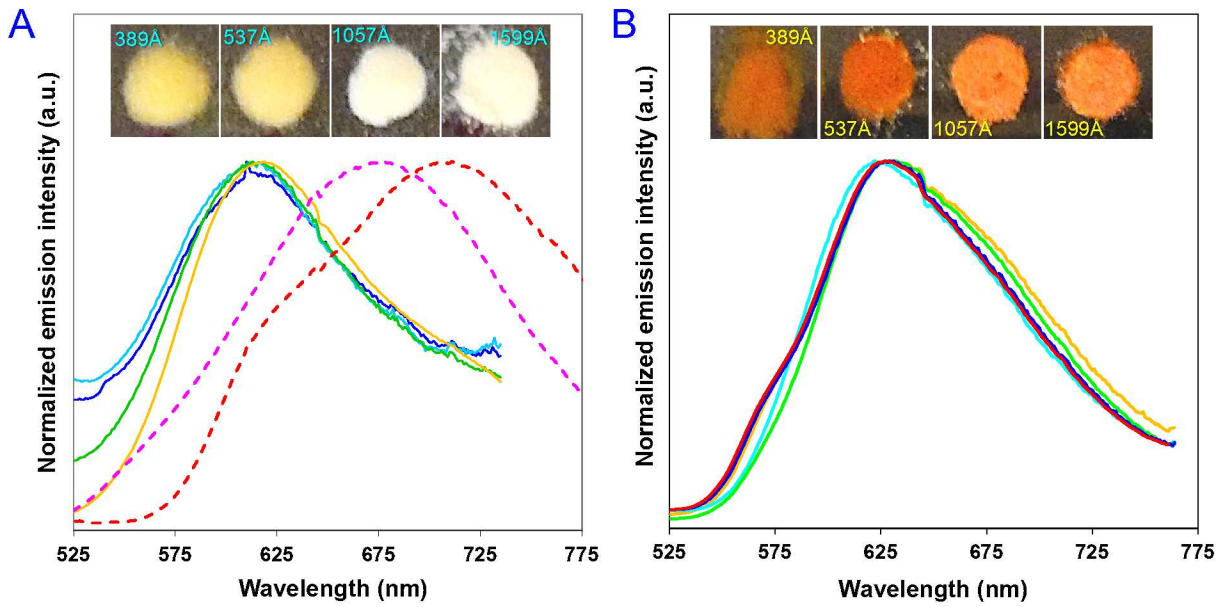

Figure 5. (A) Emsision spectra of **1**●ClO_4●H_2O (λ_{ex}=436 nm); solid lines represent **1**●ClO_4●H_2O@CPG hybrids: (—) **1**●ClO_4●H_2O@CPG-1599 Å, (—) **1**●ClO_4●H_2O@CPG-1057 Å, (—) **1**●ClO_4●H_2O@CPG-537 Å, (—) **1**●ClO_4●H_2O@CPG-383 Å; dashed lines represent the powder samples: (---) water solvated **1**●ClO_4●H_2O powder, (---) unsolvated **1**●ClO_4 powder. Inset shows the photographs of **1**●ClO_4●H_2O@CPGs. (B) Emsision spectra of **2**●Cl_2 (λ_{ex}=436 nm): (—) **2**●Cl_2@CPG-1599 Å, (—) **2**●Cl_2@CPG-1057 Å, (—) **2**●Cl_2@CPG-537 Å, (—) **2**●Cl_2@CPG-383 Å, (—) **2**●Cl_2 powder. Inset shows the photographs of **2**●Cl_2@CPGs.

Loading of the **1**●ClO_4●H_2O salt into CPGs of four different pore sizes, namely 383, 537, 1057 and 1599 Å, results in visual colorations whose color tones differ from one another by naked eye **(Figure 5(A), inset)**. However, the emission profiles of each of the **1**●ClO_4●H_2O@CPG composites upon excitation at 436 nm are characterized by a single broad emission band centered at ~620 nm **(Figure 5(A))** with no prominent changes from one another, other than variations in the width of the emission spectra. This behavior is unlike that observed in case of **1**●PF_6@CPG, where pore size was observed to make a difference. There is a significant hypsochromic shift (of about 2680 cm^{-1}) in the energy of this lowest energy emission maximum compared to the **1**●ClO_4●H_2O powders or microcrystals. This is suggestive of the destabilization of the MMLCT states due to the significant weakening of the dz^2(Pt) orbital interactions in the **1**●ClO_4●H_2O@CPGs compared to the powders, which in turn points to the weakening of the Pt•••Pt interactions upon their association with the CPGs.

To put it in context, the emission spectroscopy of unsolvated **1**●ClO_4 powders compared to the solvated **1**●ClO_4●H_2O shows a destabilization of the MMLCT in the former by only 828 cm^{-1} arisen from concurrent weakening of the Pt•••Pt interactions.[73-74] The emission energy observed for the **1**●ClO_4●H_2O@CPGs is even higher than that of the unsolvated **1**●ClO_4 powders with a destabilization of the MMLCT by 1315 cm^{-1} compared to unsolvated **1**●ClO_4 powders and by 2083cm^{-1} compared to solvated **1**●ClO_4●H_2O, suggesting the Pt•••Pt interactions in the hybrids is the weakest.

All these findings reveal a distinctly different behavior in the two square-planar platinum complexes that is induced by a combination of (i) the rigidity of the mesoporous structure of the silica framework, and (ii) the ability of the structural lattice of the parent material to accommodate Pt•••Pt interactions. **1**●PF_6 salt

shows a bathochromic shift in luminescence upon its intercalation into the silica porous structure which is due to the structural openness of the parent **1**●PF_6 units that can accommodate further enhancement in Pt•••Pt interactions. Conversely, the **1**●ClO_4●H_2O salt (for which the Pt•••Pt interactions are already present in the fullest extend and cannot be enhanced) shows a hyposochromic rigidochromism upon its association with the CPGs.

The strong hypsochromic shift in the emission energy of **1**●ClO_4●H_2O upon their association with CPGs suggest that this association disrupts the extended Pt•••Pt network. This points to a number of possibilities. This can be either (i) through a direct electronic interaction of the silica with the individual **1**●ClO_4●H_2O units that breaks the intermolecular, non-covalent Pt•••Pt interactions, or (ii) by restricting the formation of an extended Pt•••Pt network sterically. The former interaction can occur either inside the pores or on the material surface and does not require intercalation of the salt into the pores; on the other hand the latter is more likely to occur inside the silica pores upon the intercalation of the salts. This provides the motivation to probe the nature of this interaction via X-ray diffraction analysis, as discussed later.

Spectroscopic characterization of 2●Cl_2@silica.

The cumulative observations described in the previous sections indicate that the rigidity of the pores of the porous silica frameworks can influence the M•••M interactions in coordination complexes whose geometry permits such interactions. For comparisons to a control system, CPGs were also loaded with **2**●Cl_2. This complex salt has an octahedral geometry where all the six coordination sites are occupied by ligands, and therefore it is architecturally impeded from showing any M•••M interactions. The powder form of **2**●Cl_2 exhibits a broad emission band at 630 nm assigned to the luminescent deactivation from the lowest-lying ^{3}MLCT excited state.[85-86] Upon loading the complex into CPGs of pore sizes 383, 537, 1057 and 1599Å respectively, the **2**●Cl_2@CPGs show an orange coloration which are visibly indistinguishable of each of the **2**●Cl_2@CPG hybrid tested **(Figure 5(B), inset)**. The emission spectra of these four **2**●Cl_2@CPG hybrids show nearly identical feature, that is also indistinguishable from the luminescence spectrum of **2**●Cl_2 microcrystalline samples or powder **(Figure 5(B))**. While there are minute differences in emission maxima and band width, there is no systematic variation in emission features or energies, suggesting that the average emission remains practically unchanged. This suggests that the rigid pore structure of the CPGs does not impact the emission and consequently the electronic structure of **2**●Cl_2, as expected from its structural architecture.

Structural and morphological studies

X-ray diffractogram. A key consideration of our study was to determine if the chemical identities of the materials were preserved post their immobilization onto the silica supports. An added incentive was to probe any changes in the structure of the Pt(II) salt upon their interaction with silica, that was motivated by the silica induced variations in the luminescence spectra of these salts. The **1**●PF_6@CPG composites show a systematic increase in the energies of the luminescence of the **1**●PF_6@CPG composites as the CPG pore size is decreased. On the other hand, the non-variance of the luminescence spectra of **1**●ClO_4●H_2O@CPGs from each other, but the hypsochromic shift of their emission maxima from unassociated **1**●ClO_4●H_2O suggest two possibilities: (a) either they are not intercalated within the CPG pores but the change in the emission energy is a reflection of their electronic association with silica, or (b) they are intercalated within the porous silica frameworks and this intercalation results in the rigid, microporous environment of silica in all the CPGs affecting the Pt•••Pt interaction of **1**●ClO_4●H_2O in a similar way.

To characterize the identities of the materials, X-ray powder diffraction studies were performed on selected materials. For these studies, the CPG loaded materials were primarily chosen to represent the range of silica

materials. The diffractograms of the CPG materials are characterized by a broad diffraction peak centered at 21°, characteristic of polycrystalline silica (ESI **Figure S10**).

For the **1**●PF_6@CPG and **1**●ClO_4●H_2O@CPG hybrids, the diffractograms reveal a series of sharp peaks in addition to the broad peak at 21°(ESI **Figure S10 and S11**). The peak positions of the new sharp peaks and the ratio of their peak intensities are nearly identical to their starting **1**●PF_6 or **1**●ClO_4●H_2O samples, suggesting that the starting platinum salts preserve the structural integrity of their primary lattice after incorporation into the CPGs. [73-74,87] The diffractograms reveal an intriguing characteristic of the materials: the unit cell structure of both **1**●PF_6 and **1**●ClO_4●H_2O are preserved upon their association with the CPGs. While this suggests the preservation of the chemical identity post interaction of the Pt(II) salts with silica, it is counter-intuitive to their observed spectroscopies. The spectroscopies indicate significant alterations in the non-covalent Pt•••Pt interactions of the materials upon their association with silica, which is anticipated to alter the peaks in the diffractograms.

One possible explanation is that the association of the Pt(II) salts with the silica occurs at the surface only without any intercalation of the salts into the materials, and the alterations in the non-covalent Pt•••Pt interactions are caused by the surface interaction between Pt(II) and silica. However, such an explanation is unable to justify the systematic changes in the MMLCT band of the **1**●PF_6@silica composites represented in **Figures 3** & **4**, where porosity of the platform is the only variable. This suggests that the spectroscopy of the **1**●PF_6@silica is pointing towards an intercalation of **1**●PF_6 within the silica. On the other hand, the **1**●ClO_4●H_2O@CPG emission spectra can be justified based on the above explanation; these spectra show no dependence on the CPG porosity, and the variation in the energy of their MMLCT band compared to pristine **1**●ClO_4●H_2O (shown in **Figure 5(A)**) can be attributed to surface interaction of the salt with silica that does not require intercalation. However, considering that the electronic structure of the monomeric cations of **1**●PF_6 and **1**●ClO_4●H_2O are identical, and the only changes in the electronic structures of these salts are induced by the weak, non-covalent Pt•••Pt interactions, it is unlikely that these interactions are going to impact the association and intercalation of **1**●ClO_4●H_2O within silica significantly compared to **1**●PF_6. This indirectly suggests that there is possible intercalation of **1**●ClO_4●H_2O within the silica as well, and that post intercalation, the silica meso/microporous environment affects their Pt•••Pt interactions in a similar way, resulting in the observed trends in their spectroscopies.

The alternate explanation for the diffractograms of both sets **1**●PF_6@CPG and **1**●ClO_4●H_2O@CPG composites matching the respective pristine salts is that the interactions of these salts with silica affecting the long-range ordering of these materials rather than the short-range order. This change in the long-range order is reflected in the perturbations of the bulk electronic structure and spectroscopies of these materials, while the preservation of the bulk short-range structures is reflected in the diffractograms remaining invariant.

An indirect measure of the long-range order can be the relative sizes of micro crystallites. The Scherrer equation in X-ray diffraction allows one to determine the sizes of sub-micron sized crystallites in solid state from the broadening of a diffraction peak in the diffractogram using relation [1]:[88]

$$\tau = \frac{K \cdot \lambda}{\beta \cos \theta} \qquad [1]$$

where τ is the mean size of the ordered crystalline domains, K is the shape factor of the particles, λ is the X-ray wavelength, β is the line broadening at half the maximum intensity (FWHM) post subtraction of the instrumental line broadening in radians, and θ is the Bragg angle. For this work, a value of 0.9 ids used for K. For the **1**●PF_6@CPG system, the crystallite sizes were observed to be in fact dependent on the pore sizes. An inverse correlation was observed in the mean size of the **1**●PF_6 crystalline domains with the mean

CPG pore size upon intercalation of the crystallites within the CPGs. As shown in ESI **Figure S12**, as the pore size progressively increased, the mean size of the **1**●PF_6 crystalline domains decreased. On the other hand, for the **1**●ClO_4●H_2O@CPG system, the crystallite sizes of **1**●ClO_4●H_2O were observed to not be affected by the pore sizes of the CPGs. This correlation of the crystallite sizes of the two systems on their pore size, can in fact be extended to their emission spectra, as shown in ESI **Figure S13**. These observations demonstrate the impact of the matrix pororsity on the sizes of the microcrystallites, which indirectly points to the impact of the platform porosities on the long range order of the intercalated Pt(II) salts.

BET studies. BET measurements were conducted on select CPGs, both as received as well as after **1**●PF_6 or **1**●ClO_4●H_2O loading. The surface areas pre and post loading of the respective Pt(II) salts are shown in **Table 2**. A lowering of the BET surface area post-Pt(II) loading is observed for both the salts. This is suggestive of the intercalation of both the salts in the CPGs as surface deposition is unlikely to result in such consistent overall decrease in surface area. The % decrease in CPG surface area varied inversely with CPG pore size, showing an increased Pt(II) loading as the pore size decreased. These studies further validate the intercalation of both the Pt(II) salts within the CPGs. However, it is worth reiterating that in all the silica materials including the CPGs, surface deposition does take place as it is unlikely for the entire Pt(II) salt to get intercalated within the CPGs.

Table 2. Surface areas of the various CPGs measured using BET pre- and post-loading of the Pt(II) salts*

Material	Surface area (m^2g^{-1})		
	As received	Post **1**●PF_6 loading	Post **1**●ClO_4●H_2O loading
CPG-1599	20	17	16
CPG-1057	28	17	15
CPG-383	97	88	86

*Determined from N_2 sorption isotherm according to the BET model.

Scanning electron micrographs. Intrigued by the distinct variations in the luminescent spectroscopies of the **1**●PF_6@silica hybrids that were observed to depend on pore sizes, and based on the well documented studies showing the spectroscopy of **1**●PF_6 to be highly dependent on the sample preparation and history and morphology, as noted by the differences in emission energies between microcrystals[80] and powders,[78] we investigated the morphological origins of the pore-size dependent variation of **1**●PF_6@silica luminescence. SEM images were recorded to probe if there are any changes in the morphologies of the **1**●PF_6@CPG hybrids upon the variation of pore size. Representative SEM images revealed significant differences between the samples with the larger and the smaller pore sizes. Representative images of **1**●PF_6@CPG-383 shows homogeneous film like lamellar deposits on the surface of the beads (topmost panels in **Figure 6**). With increasing pore size, the homogeneity of the surface deposits was observed to progressively decrease and were being replaced by microcrystalline needles on the surface showing enhanced quantities of microcrystalline needles in the **1**●PF_6@CPG-537 and 1●PF_6@CPG-1057 hybrids. (second from top and second from bottom panels in **Figure 6**). For **1**●PF_6@CPG-1599, the needles were

observed to cover large portions of the surface (bottommost panel of **Figure 6**). It is also worth noting that lower quantities of Pt(II) salt was observed to be deposited on the surfaces of the CPGs with smaller pores compared to the larger ones. This can be speculatively approximated to represent the morphologies developed as a function of the porosity of the material, with smaller pores seemingly favoring lamellar layers and the larger pores showing dominance of needle shaped crystallites. However, it is worth noting that the morphology of the Pt(II) crystallites formed inside the rigid pores can be quite different from those formed on the free, unrestricted surface.

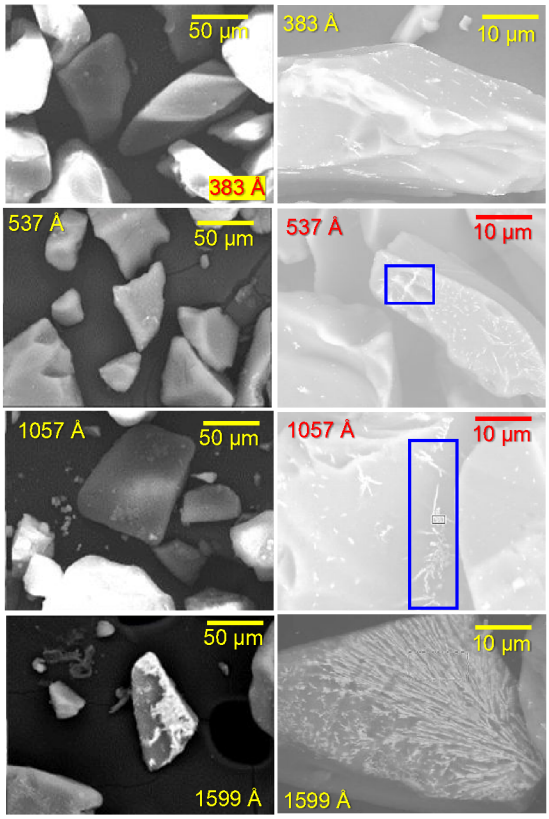

Figure 6. Representative SEM images of **1**●PF_6@CPG-383 Å (topmost panels), **1**●PF_6@CPG-537 Å (second from the top panels), **1**●PF_6@CPG-1057 Å (second from the bottom panels), **1**●PF_6@CPG-1599 Å (bottommost panels). The blue boxes represent the microcrystalline Pt(II) salt deposits on the surface.

Crystallization Morphology. The spectroscopic characterization of the **1**●PF_6@CPGs reveal a pore dependent variation in the luminescent spectra, while the microscopic studies revealed pore size dependent variations in the developed morphologies on the surface. However, it was not possible to directly take a peek into the morphologies inside the pores. Therefore, our objective was to replicate the **1**●PF_6@silica emission through crystallization of pure **1**●PF_6 material, such that the morphology of the **1**●PF_6 crystals could be tentatively assigned to that of the salt when incorporated within the pores. For these experiments, a **1**●PF_6 solution in DMSO:acetone was dropped on a microscopic slide and allowed to evaporate, as described in the experimental section. The crystal morphologies were correlated with the observed spectroscopies.

The **1**●PF_6 was observed to be completely soluble in the DMSO:acetone solvent mixture, showing a golden yellow hue. Fast drying of the solution generated a thin layer as depicted in **Figure 7 (extreme left panel)**, characterized by three general regions observed through an optical microscope, namely a thick outer ring coating characterized by larger crystallites (**region 1**), a second set of thinner concentric rings with smaller crystallites (**region 2**), while a very thin lamellar film layer is observed to extend outside of the thick ring (**region 3**). The magnified images collected under the optical microscope are shown in **Figure 7 (second from left blue panel)**,

The representative SEM images of the three regions, shown in **Figure 7 (middle orange panel)**, showed marked differences from each other. The region characterized by larger crystallites (**region 1**) showed irregular, jagged crystallites with random orientations (6 μm x 1 μm). The region characterized by thinner concentric rings demonstrated well defined needle-shaped crystals (**region 2**) (0.01x 0.01 μm), while the third region lamellar layers without any crystalline morphology (**region 3**) (2.5 x 0.2 μm).

The emission spectra (λ_{ex} = 442 nm) of the three regions show distinct differences, with both the larger crystallites with ragged, irregular architecture and the well-defined needles showing both a longer wavelength band at ~650 nm and a shorter wavelength band at ~550 nm. On the other hand, the lamellar region shows a single emission band that is significantly red shifted (centered at ~680 nm). It is to be noted that a laser source was used to record these emissions and point the beam directly on the marked spots, and therefore the excitation wavelengths were slightly different from our previous measurements. However, based on our previous observations of the emission features of **1**●PF_6@silica showing no variation upon changing the excitation wavelengths from 365 nm to 436 nm, thereby allowing the comparison of these emission spectra with those collected at a λ_{ex} of 436 nm on **1**●PF_6@silica materials.

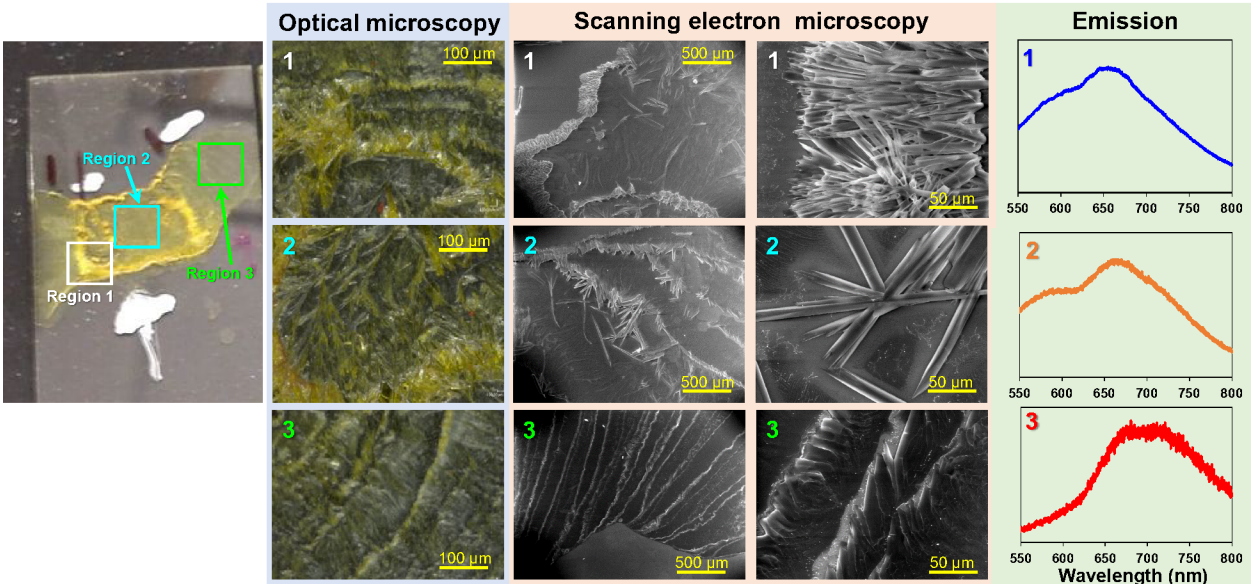

Figure 7. (extreme left panel) Photograph of a glass slide with a thin **1**●PF_6 layer deposited from a solution of DMSO:acetone under evaporation at 100°C (the regions **1**, **2** and **3** are marked, the other markings are indicators to serve as guides during emission measurements); (second from left blue panel) Representative optical microscopic images of regions **1**, **2** and **3**; (middle orange panel) representative scanning electron microscopic images of the three regions **1**, **2** and **3** at two different magnifications; (right green panel) the emission spectra of the three regions **1**, **2** and **3** upon excitation at 436 nm.

The cumulative observations indicate that as the morphology of the generated crystals changes from fine lamellar film deposits to larger crystallites with finite edges, the emission spectroscopic signature changes from one with a single low energy band to one having a companion shoulder at higher energy as well. It is possible that a similar transformation in terms of crystal size and morphology is possible in the **1**●PF_6@silica depending upon the pore sizes of the silica support. Therefore, as pore sizes are gradually reduced, the crystallite sizes get progressively reduced. In the NP-SiO_2 supports that are devoid of any pores, it is possible that the morphology is lamellar based on the similarity of the emission features. Here, we would like to note that this assumption on the morphologies is speculative, as the structural morphology withing the rigid confines of the porous framework may be entirely different from what is possible in a free, non-confined system.

CONCLUSIONS

This work reports on a relatively unexplored area where incorporation of metal complexes with sterically permitting architecture within rigid mesoporous silica frameworks generates advanced rigidochromic materials whose luminescence can be tuned by the porosity of the rigid matrix. The two chosen platinum complexes **1**●PF_6 and **1**●ClO_4●H_2O exhibits a rich expanse of rigidochromic behavior. In the **1**●PF_6 case, the pore rigidity enforces the otherwise discrete **1**●PF_6 dimeric units into closer contact than the free powder form. This enhances the interaction of the d_{z2}(Pt) orbitals of the adjacent square-planar units and stabilizes the MMLCT transition. This is reflected in a bathochromic shift in luminescent energy upon intercalation of the material into the silica pores, the smaller the pore size the greater the shift.

At the other extreme, in the **1**●ClO_4●H_2O case, its intercalation into the silica pores disrupts the extended Pt•••Pt interaction network that is present in the free powder form. This is presumably due to the rigidity enforced by the pore geometry which may not be suited for the extended long-range structure with extensive Pt•••Pt interactions that is possible in the unrestricted powder form. The pore geometry and structural rigidity likely leads to the reorientation of the individual $[Pt(tpy)Cl]^+$ units, which may not accommodate the extended dz^2(Pt) orbital interactions that was possible in the free form. This destabilizes the lowest energy MMLCT, which is reflected in a hyposochromic shift in luminescent energy of **1**●ClO_4●H_2O upon its intercalation within the silica supports.

This rigidochromic effect is likely to be observed in materials whose architecture consists of accessible axial sites, therefore in rigid structures whose geometry stays unperturbed in presence of perturbations in matrix effects and structural rigidity as in the case of the **2**●Cl_2@CPGs, no effect was observed.

For the **1**●PF_6@silica hybrids, linear dependences were observed between pore size and the semi-logarithm of the intensity ratios of the 550 nm emission band relative to the one around 650 nm (i.e. pore size α $\log(I_{550\ nm}/I_{650\ nm})$ or pore size and intensity ratios of the ~448 nm to the ~368 nm excitation bands (i.e. pore size α $I_{448\ nm}/I_{368\ nm}$). These studies demonstrate the potential applicability of other similar rigidochromic platinum salts an a new class of advanced sensing materials for rapid, economic, *in-situ* quantitative assesment of silica pore sizes. Future studies will be invested to assess the sensitivity of the process and in expanding the applicability of the technique to assess porosities of other engineered systems that are used for various practical applications.[82, 88-90]

X-ray diffraction studies provide evidence that the interaction of platinum salts with the silica supports impacts and perturbs the long range structural order while preserving the short range structure. In summary, this work provides the motivation for more comprehensive investigation of these hybrid materials. The integration of photoluminescent rigidochromic materials with other porous frameworks can provide wider

applications in the areas of sensing of emerging contaminants, as well as photocatalytic and photosensitization applications.

EXPERIMENTAL SECTION

Reagents and Materials.

Dimethyl sulfoxide (DMSO), terpyridine (tpy), 1,5-cyclooctadiene (COD), Dimethylformamide (DMF) and acetone was purchased from Sigma Aldrich. K_2PtCl_4 and **2**●Cl_2 complexes was purchased from Pressure Chemical Company. **1**●PF_6 was prepared according to published procedures.[71] CPGs with six different pore sizes (383 Å, 537 Å, 623 Å, 815 Å,1057 Å and 1599) were purchased from Prime Synthesis. CPGs with pore size 70 Å were purchased from Millipore. MCM-41 and NP-SiO_2 were purchased from sigma Aldrich.

Incorporation of materials into CPGs.

Cleaning of CPGs. CPG beads were cleaned thoroughly before loading to ensure no contamination or blockages were present in the pores pre material loading. A solution of 1:1 HCl:MeOH was added to a weighted amount of CPGs in the ratio of 0.5mL/ 0.1 g, and the resultant mixture was allowed to sit for 30 minutes. The solution was decanted off, and the beads were washed by rinsing with water 5 times. Subsequently, they were dried by heating in an oven at 125^0F and dried for 24 hours.

Incorporation of 1●PF_6 **into CPGs (1**●**PF_6@CPGs).**
Acetone:DMSO procedure. A 2 weight % (m/m) solution of **1**•PF_6 was prepared in a 1:1 mixture of Acetone:DMSO. The solution was sonicated for 30 minutes and 0.5 mL of the solution was added to 0.1 grams of each of the CPGs (70, 383, 537 1057, 1599Å). The resultant **1**•PF_6@CPGs were allowed to dry for 12 hours at 100°C.
Acetone/Water Procedure. A 2 weight % (m/m) mixture of **1**•PF_6 was prepared in a 1:1 mixture of Acetone:water. This created a slurry. The slurry was sonicated for 30 minutes and 0.5 mL of the solution was added to 0.1 grams of each of the CPGs (383, 1057, 1599Å). The resultant **1**•PF_6@CPGs were allowed to dry for 12 hours at 100°C.

Incorporation of 1●ClO_4●H_2O **into CPGs (1**●**ClO_4**●**H_2O@CPGs).** A 2 weight % (m/m) solution of **1**•ClO_4 was prepared in a 1:1 mixture of Acetone:DMSO. The solution was sonicated for 30 minutes and 0.5 mL of the solution was added to 0.1 grams of each of the CPGs (383, 537 1057, 1599Å). The resultant **1**•ClO_4@CPGs were allowed to dry for 12 hours at 100°C.

Incorporation of 2●Cl_2 **into CPGs (2**●**Cl_2@CPGs).** A 2 weight % (m/m) solution of **2**●Cl_2 was prepared in a 1:1 mixture of Acetone:water. **2**●Cl_2 fully dissolves in acetone:water. The solution was sonicated for 30 minutes and 0.5 mL of the solution was added to 0.1 grams of each of the CPGs (383, 537, 1057, 1599Å). The resultant **2**●Cl_2@CPGs were allowed to dry for 12 hours at 100°C.

Incorporation of materials into or on other substrates
MCM-41(1●PF_6@**MCM-41).** A 2 weight % (m/m) solution of **1**•PF_6 was prepared in a 1:1 mixture of Acetone:DMSO. The solution was sonicated for 30 minutes and 0.5 mL of the solution was added to 0.1 MCM-41. The resultant **1**•PF_6@MCM-41 were allowed to dry for 12 hours at 100°C.

NP-SiO_2 (1●PF_6@NP-SiO_2). A 2 weight % (m/m) solution of **1**•PF_6 was prepared in a 1:1 mixture of Acetone:DMSO. The solution was sonicated for 30 minutes and 0.5 mL of the solution was added to NP-SiO_2. The resultant **1**•PF_6@ NP-SiO_2 was allowed to dry for 12 hours at 100°C.

Thin Films on silica slides

A 2% solution (w/w) of **1**●PF_6 in DMSO/acetone or water/acetone was prepared on glass microscope slides where prepare. 1 mL of the solution was then dropped to a hot microscope slide at 100°C and was allowed to evaporate. Mass spectroscopy (Fig. S1) and ^{1}HNMR of the slides showed matching spectrum to the **1**●PF_6.

Emission Measurements

For emission measurements of **1**●PF_6, **1**●ClO_4●H_2O and **2**●Cl_2@silica, a thin layer of vacuum grease was applied to a microscope slide. 0.02 g of silica loaded with the appropriate Pt(II)/Ru(II) salt were added to the microscope slide. The excess material was removed by tapping the slides 4 times. For measurements of **1**●PF_6 thin films, the films were used as is.

Characterization and Methods.

Room-temperature steady-state emission and excitation spectra were collected using a SPEX Fluorolog-3 fluorimeter equipped with a double emission monochromator and a single excitation monochromator. Scanning electron microscopy measurements were carried out using a FEI XL-30 environmental scanning electron microscope (ESEM). The samples were not coated with metal. Secondary-emission electron images were collected using 15 kV accelerating potential and a 5.6 μm spot size. Optical videos of crystals on slides were taken using a Keyence Digital Microscope VHX-1000 at 1000xs.

Specific surface area determination was performed by recording nitrogen sorption isotherms at 77 K with a Micromeritics ASAP2010 equipment (Micromeritics Corp., Norcross, GA, USA) after degassing each sample at 150°C in vacuum for a time interval long enough to reach a constant pressure (<10 μm Hg). The BET equation was then applied between 0.01 and 0.3 relative pressure (P/P_0) to calculate the specific surface areas S_{BET}. SEM images were recorded with a HITACHI TM-1000 table microscope. Powder X-ray diffraction (XRD) measurements were performed on impregnated sample with a Bruker AXS diffractometer (D2 Phaser A26-X1-A2B0D3A) with a Cu K_α line of 0.154184 nm.

^{1}H NMR spectra were recorded at room temperature using a Bruker AC 400 MHz NMR. Optical images were recorded using a Keyence Digital Microscope VHX-1000 with timer recording. Mass spectra were obtained using a Micromass Q-Tof 2 (Waters, Milford, MA, USA). The mass spectrometer was calibrated in positive ion mode using poly-alanine (Sigma, St. Louis, MO, USA) and in negative ion mode using sodium iodide (Fisher Scientific). The observed isotope patterns agreed well with those predicted based on natural isotopic abundances.

ASSOCIATED CONTENT

Supporting Information

Mass spectrum of **1**●PF_6 post its deposition as a thin film; photographs of **1**●PF_6 solutions and the CPGs pre **1**●PF_6 loading, and **1**●PF_6@CPGs post loading; emission spectra of **1**●PF_6@silica compared to pristine

1●PF_6; emission spectra of **1**●PF6@CPGs excited at different wavelengths; normalized excitation spectra of **1**●PF_6@CPGs monitored at λ_{em} = 550 nm; emission spectra of **1**●PF_6@CPGs over 3 cycles of **1**●PF_6 loading onto the CPGs; emission spectra of **1**●PF_6@CPGs based on drying times post **1**●PF_6 loading; emission spectra of **1**●PF_6@CPGs with different solvents used for **1**●PF_6 loading; emission spectra of **1**●PF_6@CPGs (λ_{ex} = 436 nm) recorded at different times; X-ray powder diffractograms of **1**●PF_6@CPGs; X-ray powder diffractograms of **1**●ClO_4●H_2O@CPGs; plot of the mean size of the ordered crystalline domains calculated using Scherrer equation versus the mean pore sizes of the CPGs; plot of the ratios of the intensity ratios of the ~550 nm and the ~650 nm emission bands for **1**●PF_6@CPGs (λ_{ex}=436 nm) versus the mean size of the ordered crystalline domains.

CONFLICTS OF INTEREST

"There are no conflicts to declare".

ACKNOWLEDGEMENTS

This work was supported by STAR Fellowship Assistance Agreement FP-91765901 awarded by the U.S. Environmental Protection Agency (EPA) (A.E.N.), and the National Science Foundation (CHE-1152853) (W.B.C.). A.S.S.C. acknowledges support from Conselho Nacional de Desenvolvimento Científico e Tecnológico (CNPq), Project 402011/2016-3, and the Center for Research, Technology and Education in Vitreous Materials (CeRTEV), Project 2013/07793-6, funded by Fundação de Amparo à Pesquisa do Estado de São Paulo (FAPESP), which also granted scholarships to K.P.S.Z. for post-doctorate (Grant Number 2016/07706-4) and research internships abroad (Grant Number 2018/05152-7) L.P.R. is also thankful to CNPq for a postdoctoral scholarship (152438/2018-1).

REFERENCES

1. Rivera, E. J.; Barbosa, C.; Torres, R.; Rivera, H.; Fachini, E. R.; Green, T. W.; Connick, W. B.; Colón, J. L. Luminescence Rigidochromism and Redox Chemistry of Pyrazolate-Bridged Binuclear Platinum(II) Diimine Complex Intercalated into Zirconium Phosphate Layers. *Inorg. Chem.* **2012**, *51*(5), 2777-2784.
2. Jamwal, H. S.; Ranote, S.; Kumar, D.; Chauhan, G. S.; Bansal, M. Gelatin-based Mesoporous Hybrid Materials for Hg^{2+} ions Removal from Aqueous Solutions. *Sep. Purif. Technol.* **2020,** *239*, 116513.
3. Bordoni, A. V.; Zalduendo, M. M.; Escobar, A.; Amenitsch, H.; Moya, S. E.; Angelomé, P. C. Phosphonate Mesoporous Hybrid Thin Films: Synthesis of Organophosphosilane by Thiol-ene Click Chemistry and Applications Information and Stabilization of Silver Nanoparticles. *Microporous Mesoporous Mater.* **2020,** *295*, 109958.
4. Chahrour, K. M.; Yam, F.; Eid, A.; Nazeer, A. A. Enhanced Photoelectrochemical Properties of Hierarchical Black TiO_2-x Nanolaces for Cr(VI) Photocatalytic Reduction. *Inter. J. Hydrogen Energy* **2020,** *45*(43), 22674-22690.
5. Qiao, X.; Wang, C.; Niu, Y. N-Benzyl HMTA Induced Self-assembly of Organic-Inorganic Hybrid Materials for Efficient Photocatalytic Degradation of Tetracycline. *J. Hazard. Mater.* **2020,** *391*, 122121.
6. Sun, M.; Li, Z.; Fang, Q.; Han, S.; Cai, C.; Li, H.; Shen, W.; Liu, X.; Fu, Y. Room-temperature Synthesized Porous $Cu(OH)_2/Cu_7S_4$ Hybrid Nanowires as a High-Performance Electrode Material for Asymmetric Supercapacitors. *J. Mater. Chem. A* **2020,** *8*(2), 724-734.
7. Garcia, Y.; Su, B. L. No Inorganic Materials, No Progress. *Eur. J. Inorg. Chem.* **2019,** *27*, 3123-3125.

8. Rivera, E. J.; Figueroa, C.; Colón, J. L.; Grove, L.; Connick, W. B. Room-temperature Emission from Platinum(II) Complexes Intercalated into Zirconium Phosphate-layered Materials. *Inorg. Chem.* **2007,** *46*(21), 8569-8576.
9. Rivera, E. J.; Barbosa, C.; Torres, R.; Grove, L.; Taylor, S.; Connick, W. B.; Clearfield, A.; Colón, J. L. Vapochromic and Vapoluminescent Response of Materials based on Platinum(II) Complexes Intercalated into Layered Zirconium Phosphate. *J. Mater. Chem.* **2011,** *21*(40), 15899-15902.
10. Mädler, L.; Roessler, A.; Pratsinis, S. E.; Sahm, T.; Gurlo, A.; Barsan, N.; Weimar, U. Direct Formation of Highly Porous Gas-sensing Films by Insitu Thermophoretic Deposition of Flame-made Pt/SnO_2 Nanoparticles. *Sens. Actuators, B.* **2006,** *114*(1), 283-295.
11. Shukla, S.; Priscilla, A.; Banerjee, M.; Bhonde, R. R.; Ghatak, J.; Satyam, P.; Sastry, M. Porous Gold Nanospheres by Controlled Transmetalation Reaction: a Novel Material for Application in Cell Imaging. *Chem. Mater.* **2005,** *17*(20), 5000-5005.
12. Siepmann, J.; Siegel, R. A.; Rathbone, M. J., *Fundamentals and Applications of Controlled Release Drug Delivery*. Springer 2012; Vol. 3.
13. Ammari, F.; Lamotte, J.; Touroude, R. An Emergent Catalytic Material: Pt/ZnO Catalyst for Selective Hydrogenation of Crotonaldehyde. *J. Catal.* **2004,** *221*(1), 32-42.
14. Mori, K.; Watanabe, K.; Kawashima, M.; Che, M.; Yamashita, H. Anchoring of Pt(II) Pyridyl Complex to Mesoporous Silica Materials: Enhanced Photoluminescence Emission at Room Temperature and Photooxidation Activity using Molecular Oxygen. *J. Phys. Chem. C* **2011,** *115*(4), 1044-1050.
15. Mori, K.; Watanabe, K.; Terai, Y.; Fujiwara, Y.; Yamashita, H. Hybrid Mesoporous-Silica Materials Functionalized by Pt(II) Complexes: Correlation between the Spatial Distribution of the Active Center, Photoluminescence Emission, and Photocatalytic Activity. *Chem.Eur. J.* **2012,** *18*(36), 11371-11378.
16. Chatterjee, S.; Krause, J. A.; Oliver, A. G.; Connick, W. B. Intramolecular NH···Pt Interactions of Platinum(II) Diimine Complexes with Phenyl Ligands. *Inorg. Chem.* **2010,** *49*(21), 9798-9808.
17. Kuyuldar, S.; Burda, C.; Connick, W. B. Tuning Two-Electron Transfer in Terpyridine-based Platinum(II) Pincer Complexes. *RSC Adv.* **2019,** *9*(37), 21116-21124.
18. Chatterjee, S.; Krause, J. A.; Madduma-Liyanage, K.; Connick, W. B. Platinum(II) Diimine Complexes with Halide/Pseudohalide Ligands and Dangling Trialkylamine or Ammonium Groups. *Inorg. Chem.* **2012,** *51*(8), 4572-4587.
19. Jude, H.; Krause Bauer, J. A.; Connick, W. B. An Outer-Sphere Two-Electron Platinum Reagent. *J. Am. Chem. Soc.* **2003,** *125*(12), 3446-3447.
20. Nikol, H.; Bürgi, H.-B.; Hardcastle, K. I.; Gray, H. B. Syntheses and Structures of the Five-Coordinate Complexes $[M(NN)([9]aneS_3)](PF_6)_2$ (M= Pd,(NN)= 2, 2'-Bipyridine; M= Pt,(NN)= 1, 10-Phenanthroline;([9] $aneS_3$)= 1, 4, 7-Trithiacyclononane). *Inorg. Chem.* **1995,** *34*(25), 6319-6322.
21. Koo, C.-K.; Lam, B.; Leung, S.-K.; Lam, M. H.-W.; Wong, W.-Y. A "Molecular Pivot-Hinge" Based on the pH-Regulated Intramolecular Switching of Pt− Pt and π− π Interactions. *J. Am. Chem. Soc.* **2006,** *128*(51), 16434-16435.
22. Prokopchuk, E. M.; Jenkins, H. A.; Puddephatt, R. J. Stable Cationic Dimethyl (hydrido) Platinum(IV) Complex. *Organometallics* **1999,** *18*(15), 2861-2866.
23. Blake, A. J.; Schröder, M. Chemistry of Thioether Macrocyclic Complexes. *Adv. Inorg. Chem*, 1990; *35*,1-80.
24. Chatterjee, S.; Krause, J. A.; Connick, W. B.; Genre, C.; Rodrigue-Witchel, A.; Reber, C. Interaction of $SbCl_5^{2-}$ and Thioether Groups at the Open Coordination Sites of Platinum(II) Diimine Complexes. *Inorg. Chem.* **2010,** *49*(6), 2808-2815.
25. Abdolmaleki, M. K.; Riasi, M. S.; Enayati, M.; Norton, A. E.; Chatterjee, S.; Yeghiazarian, L.; Connick, W. B.; Abbaspourrad, A. A Digital Imaging Method for Evaluating the Kinetics of Vapochromic Response. *Talanta* **2020,** *209*, 120520.

26. Norton, A. E.; Abdolmaleki, M. K.; Liang, J.; Sharma, M.; Golsby, R.; Zoller, A.; Krause, J. A.; Connick, W. B.; Chatterjee, S. Phase Transformation Induced Mechanochromism in a Platinum Salt: A Tale of Two Polymorphs. *Chem. Commun,* **2020**, *56*, 10175-10178.
27. Chatterjee, S. ; Norton, A. E. ; Edwards, M. K.; Peterson, J. M.; Taylor, S. D. ; Bryan, S. D.; Andersen, A. ; Govind, N.; Albrecht-Schmitt, T. E.; Connick, W. B. ; Levitskaia, T. G. Highly Selective Colorimetric and Luminescence Sensing of Aqueous TcO_4^- using a Square-Planar Platinum(II) Terpyridal Complex. *Inorg. Chem.* **2015,** *54*(20), 9914-9923.
28. Garakyaraghi, S.; Castellano, F. N. Nanocrystals for Triplet Sensitization: Molecular Behavior from Quantum-confined Materials. *Inorg. Chem.* **2018,** *57*(5), 2351–2359
29. Norton, A. E.; Abdolmaleki, M. K.; Ringo, J. M.; Shingade, V. M.; Cashen, C.; Sharma, M.; Connick, W. B.; Chatterjee, S. A Colorimetric/luminescence Sensor for Detecting MeCN in Water: Towards Direct Detection of Dissolved Organic Contaminants. *Sens. Actuators B* **2021,** *329*, 129207.
30. Norton, A. E.; Sharma, M.; Cashen, C.; Dourges, M.; Toupance, T.; Krause, J.; Motkuri, R.; Connick, W. B.; Chatterjee, S. pH Mediated Colorimetric and Luminescent Sensing of Aqueous Nitrate Anions by a Platinum(II) Luminophore@Mesoporous Silica Composite. *ACS Appl. Mater. Inter.* **2021,** *ASAP*.
31. Zhao, W.; Sun, Y.; Castellano, F. N. Visible-Light Induced Water Detoxification Catalyzed by Pt(II) Dye Sensitized Titania. *J. Am. Chem. Soc.* **2008,** *130*(38), 12566-12567.
32. Muro, M. L.; Daws, C. A.; Castellano, F. N. Microarray Pattern Recognition based on Pt(II) Terpyridyl Chloride Complexes: Vapochromic and Vapoluminescent Response. *Chem. Commun.* **2008,** *46*, 6134-6136.
33. Matsukawa, H.; Yoshida, M.; Tsunenari, T.; Nozawa, S.; Sato-Tomita, A.; Maegawa, Y.; Inagaki, S.; Kobayashi, A.; Kato, M. Fast and Stable Vapochromic Response Induced through Nanocrystal Formation of a Luminescent Platinum (II) Complex on Periodic Mesoporous Organosilica. *Sci. Rep.* **2019,** *9*, 15151.
34. Kato, M.; Ito, H.; Miki Hasegawa, P.; Ishii, K. Soft Crystals: Flexible Response Systems with High Structural Order. *Chem. Eur. J.* **2019,** *25*(20), 5105-5112.
35. Li, Y.; Chen, L.; Ai, Y.; Hong, E. Y.-H.; Chan, A. K.-W.; Yam, V. W.-W. Supramolecular Self-assembly and Dual-switch Vapochromic, Vapoluminescent, and Resistive Memory Behaviors of Amphiphilic Platinum(II) Complexes. *J. Am. Chem. Soc.* **2017,** *139*(39), 13858-13866.
36. Yam, V. W.-W.; Au, V. K.-M.; Leung, S. Y.-L. Light-Emitting Self-assembled Materials based on d8 and d10 Transition Metal Complexes. *Chem. Rev.* **2015,** *115*(15), 7589-7728.
37. Kobayashi, A.; Kato, M. Vapochromic Platinum (II) Complexes: Crystal Engineering toward Intelligent Sensing Devices. *Eur. J. Inorg. Chem.* **2014,** *27*, 4469-4483.
38. Feng, K.; Peng, M.-L.; Wang, D.-H.; Zhang, L.-P.; Tung, C.-H.; Wu, L.-Z. Silica- and Polymer-Supported Platinum(II) Polypyridyl Complexes: Synthesis and Application in Photosensitized Oxidation of Alkenes. *Dalton Trans.* **2009,** 44, 9794-9799.
39. Chen, Y. L.; Spiering, A. J. H.; Karthikeyan, S.; Peters, G. W. M.; Meijer, E. W.; Sijbesma, R. P. Mechanically induced Chemiluminescence from Polymers Incorporating a 1,2-Dioxetane Unit in the Main Chain. *Nat. Chem.* **2012,** *4*(7), 559-562.
40. Zhang, H.; Zeng, D.; Pan, Y.; Chen, Y.; Ruan, Y.; Xu, Y.; Boulatov, R.; Creton, C.; Weng, W. Mechanochromism and Optical Remodeling of Multi-network Elastomers Containing Anthracene Dimers. *Chem. Sci.* **2019,** *10*(36), 8367-8373.
41. Atoini, Y.; Prasetyanto, E. A.; Chen, P.; Silvestrini, S.; Harrowfield, J.; De Cola, L. Luminescence of Amphiphilic Pt(II) Complexes Controlled by Confinement. *Chem. Eur. J.* **2018,** *24*(46), 12054-12060.
42. Jobbagy, C.; Deak, A., Stimuli-Responsive Dynamic Gold Complexes. *Eur. J. Inorg. Chem.* **2014,** *27*, 4434-4449.
43. Che, C.-M.; Fu, W.-F.; Lai, S.-W.; Hou, Y.-J.; Liu, Y.-L. Solvatochromic Response Imposed by Environmental Changes in Matrix/chromophore Entities: Luminescent Cyclometalated Platinum(II) Complex in Nafion and Silica Materials. *Chem. Commun.* **2003,** *1*, 118-119.

44. Grove, L. J. Synthesis and Characterization of Vapochromic Platinum(II) Complexes. University of Cincinnati, 2007.
45. Pucci, A.; Ruggeri, G. Mechanochromic Polymer Blends. *J. Mater. Chem.* **2011,** *21*(23), 8282-8291.
46. Kumpfer, J. R.; Taylor, S. D.; Connick, W. B.; Rowan, S. J. Vapochromic and Mechanochromic Films from Square-planar Platinum Complexes in Polymethacrylates. *J. Mater. Chem.* **2012,** *22*(28), 14196-14204.
47. Peterson, G. I.; Larsen, M. B.; Ganter, M. A.; Storti, D. W.; Boydston, A. J. 3D-Printed Mechanochromic Materials. *ACS Appl. Mater. Inter.* **2015,** *7*(1), 577-583.
48. Achira, H.; Hoga, Y.; Yoshikawa, I.; Mutai, T.; Matsumura, K.; Houjou, H. Effects of a Semiflexible Linker on the Mechanochromic hotoluminescence of bis (Pt-salen) Complex. *Polyhedron* **2016,** *113*, 123-131.
49. Reber, C.; Sonneville, C.; Poirier, S.; Bélanger-Desmarais, N.; Connick, W. B.; Chatterjee, S.; Franz, P.; Decurtins, S. Variable-pressure Luminescence and Raman Spectroscopy of Molecular Transition Metal Complexes: Spectroscopic Effects Originating from Small, Reversible Structural Variations. *RSC Specialist Periodical Reports: Spectroscopic Properties of Inorganic and Organometallic Compounds,*. **2014,** *45*, 260-273.
50. Shigeta, Y.; Kobayashi, A.; Ohba, T.; Yoshida, M.; Matsumoto, T.; Chang, H. C.; Kato, M. Shape-Memory Platinum (II) Complexes: Intelligent Vapor-History Sensor with ON–OFF Switching Function. *Chem. Eur. J.* **2016,** *22*(8), 2682-2690.
51. Lee, W. W. S.; Wong, K. Y.; Li, X. M. Luminescent Dicyanoplatinum(II) Complexes as Sensors for the Optical Measurement of Oxygen Concentrations. *Anal. Chem.* **1993,** *65*(3), 255-258.
52. Dourado, S.; Kopelman, R. Development of Fluorescent Fiber-optic Single Polymer Membrane Sensors for Simultaneous Ratiometric Detection of Oxygen and Carbon Dioxide in Biological Systems. *Proceedings of SPIE-The International Society for Optical Engineering* **1999,** *3540* (Chemical, Biochemical, and Environmental Fiber Sensors X), 224-234.
53. Zhang, D.; Wu, L.-Z.; Yang, Q.-Z.; Li, X.-H.; Zhang, L.-P.; Tung, C.-H. Versatile Photosensitization System for $^1O_2$-Mediated Oxidation of Alkenes Based on Nafion-Supported Platinum(II) Terpyridyl Acetylide Complex. *Org. Lett.* **2003,** *5*(18), 3221-3224.
54. Tong, Q.-X.; Li, X.-H.; Wu, L.-Z.; Yang, Q.-Z.; Zhang, L.-P.; Tung, C.-H. Nafion-induced Metal-metal Interactions in a Platinum(II) Terpyridyl Acetylide Complex: A Luminescent Sensor for Detection of Volatile Organic Compounds. *Chin. J. Chem.* **2004,** *22*(10), 1204-1207.
55. Chu, C.-S.; Lo, Y.-L. 2D full-field Measurement of Oxygen Concentration Based on the Phase Fluorometry Technique that uses the Four-Frame Integrating-Bucket Method. *Sens. Actuators, B* **2010,** *147*(1), 310-315.
56. Wang, B.; Zhang, L.; Li, B.; Li, Y.; Shi, Y.; Shi, T. Synthesis, Characterization, and Oxygen Sensing Properties of Functionalized Mesoporous Silica SBA-15 and MCM-41 with a Pt(II)-porphyrin Complex. *Sens. Actuators, B* **2014,** *190*, 93-100.
57. Stich, M. I. J.; Nagl, S.; Wolfbeis, O. S.; Henne, U.; Schaeferling, M. A Dual Luminescent Sensor Material for Simultaneous Imaging of Pressure and Temperature on Surfaces. *Adv. Funct. Mater.* **2008,** *18*(9), 1399-1406.
58. Nishiyama, N.; Kato, Y.; Sugiyama, Y.; Kataoka, K. Cisplatin-Loaded Polymer-Metal Complex Micelle with Time-Modulated Decaying Property as a Novel Drug Delivery System. *Pharm. Res.* **2001,** *18*(7), 1035-1041.
59. Che, C.-M.; Zhang, J.-L.; Lin, L.-R. PEG-Linked Luminescent Platinum(II) Complex as Aqueous Polymeric Molecular Light Switch for Protein Binding Reactions. *Chem. Commun.* **2002,** *21*, 2556-2557.
60. Parrinello, G.; Stille, J. K. Asymmetric Hydroformylation Catalyzed by Homogeneous and Polymer-supported Platinum Complexes Containing Chiral Phosphine Ligands. *J. Am. Chem. Soc.* **1987,** *109*(23), 7122-7127.

61. Abe, T.; Takahashi, K.; Shiraishi, Y.; Toshima, N.; Kaneko, M. An Active Catalyst System for Proton Reduction Composed of a Bipyridyl Platinum Complex and a Polymer Membrane. *Macromol. Chem. Phys.* **2000,** *201*(1), 102-106.
62. Yang, Y.; Zhang, D.; Wu, L.-Z.; Chen, B.; Zhang, L.-P.; Tung, C.-H. Photosensitized Oxidative Deprotection of Oximes to their Corresponding Carbonyl Compounds by Platinum(II) Terpyridyl Acetylide Complex. *J. Org. Chem.* **2004,** *69*(14), 4788-4791.
63. Chow, P.-K.; Cheng, G.; Tong, G. S. M.; To, W.-P.; Kwong, W.-L.; Low, K.-H.; Kwok, C.-C.; Ma, C.; Che, C.-M. Luminescent Pincer Platinum(II) Complexes with Emission Quantum Yields up to Almost Unity: Photophysics, Photoreductive CC Bond Formation, and Materials Applications. *Angew. Chem., Int. Ed.* **2015,** *54*(7), 2084-2089.
64. Feng, K.; Zhang, R.-Y.; Wu, L.-Z.; Tu, B.; Peng, M.-L.; Zhang, L.-P.; Zhao, D.; Tung, C.-H. Photooxidation of Olefins under Oxygen in Platinum(II) Complex-Loaded Mesoporous Molecular Sieves. *J. Am. Chem. Soc.* **2006,** *128*(45), 14685-14690.
65. Feng, K.; Wu, L.-Z.; Zhang, L.-P.; Tung, C.-H. IRA-200 Resin-supported Platinum(II) Complex for Photooxidation of Olefins. *Tetrahedron* **2007,** *63*, 4907-4911.
66. Zhang, H.; Sun, Y.; Ye, K.; Zhang, P.; Wang, Y. Oxygen Sensing Materials based on Mesoporous Silica MCM-41 and Pt(II)–porphyrin Complexes. *J. Mater. Chem.* **2005,** *15*(31), 3181-3186.
67. Wang, B.; Zhang, L.; Li, B.; Li, Y.; Shi, Y.; Shi, T. Synthesis, Characterization, and Oxygen Sensing Properties of Functionalized Mesoporous Silica SBA-15 and MCM-41 with a Pt(II)–porphyrin complex. *Sens. Actuators B* **2014,** *190*, 93-100.
68. Che, C.-M.; Fu, W.-F.; Lai, S.-W.; Hou, Y.-J.; Liu, Y.-L. Solvatochromic Response Imposed by Environmental Changes in Matrix/chromophore Entities: Luminescent Cyclometalated Platinum(II) Complex in Nafion and Silica Materials. *Chem. Commun.* **2003,** *1*, 118-119.
69. Lees, A. J. The Luminescence Rigidochromic Effect Exhibited by Organometallic Complexes: Rationale and Applications. *Comments Inorg. Chem.* **1995,** *17*(6), 319-346.
70. Song, B.; Kim, J.; Chung, I.; Yun, Y. Mesoporous Silica-supported Pt Catalysts in Enantioselective Hydrogenation of Ethyl Pyruvate. *Catal. Today* **2020**, *ASAP*, doi.org/10.1016/j.cattod.2020.06.010
71. Bailey, J. A.; Hill, G. M.; Marsh, R. E.; Miskowski, V. M.; Schaefer, W. P.; Gray, H. B. Electronic Spectroscopy of Chloro(terpyridine)platinum(II). *Inorg. Chem.* **1995,** *34*(18), 4591-4599.
72. Zhang, R.; Liang, Z.; Han, A.; Wu, H.; Du, P.; Lai, W.; Cao, R. Structural, Spectroscopic and Theoretical Studies of a Vapochromic Platinum (II) Terpyridyl Complex. *CrystEngComm* **2014,** *16*(25), 5531-5542.
73. Taylor, S. D.; Howard, W.; Kaval, N.; Hart, R.; Krause, J. A.; Connick, W. B. Solid-state Materials for Anion Sensing in Aqueous Solution: Highly Selective Colorimetric and Luminescence-based Detection of Perchlorate using a Platinum(II) Salt. *Chem. Commun.* **2010,** *46*, 1070-1072.
74. Taylor, S. D.; Norton, A. E.; Hart, R. T.; Abdolmaleki, M. K.; Krause, J. A.; Connick, W. B. Between Red and Yellow: Evidence of Intermediates in a Vapochromic Pt(II) Salt. *Chem. Commun.* **2013,** *49*, 9161-9163.
75. Ferguson, J.; Herren, F.; Krausz, E.; Maeder, M.; Vrbancich, J., Electronic spectroscopy of M $(bpy)^{2+}_3$ (M= Fe, Ru, Os), Cr$(bpy)^{3+}_3$ and related compounds. *Coord. Chem. Rev.* **1985,** *64*, 21-39.
76. Shingade, V. M.; Grove, L. J.; Connick, W. B. Luminescent Pt(2, 6-bis (N-methylbenzimidazol-2-yl) pyridine)X^+: A Comparison with the Spectroscopic and Electrochemical Properties of Pt(tpy)X^+(X= Cl, CCPh, Ph, or CH_3). *Dalton Trans.* **2020,** *49(28),* 9651-9661
77. Wang, S. F.; Fu, L.-W.; Wei, Y.-C.; Liu, S.-H.; Lin, J.-A.; Lee, G.-H.; Chou, P.-T.; Huang, J.-Z.; Wu, C.-I.; Yuan, Y. Near-Infrared Emission Induced by Shortened Pt–Pt Contact: Diplatinum (II) Complexes with Pyridyl Pyrimidinato Cyclometalates. *Inorg. Chem.* **2019,** *58*(20), 13892-13901.
78. Bailey, J. A.; Miskowski, V. M.; Gray, H. B. Spectroscopic and Structural Properties of Binuclear Platinum-terpyridine Complexes. *Inorg. Chem.* **1993,** *32*(4), 369-370.

79. Yip, H.-K.; Cheng, L.-K.; Cheung, K.-K.; Che, C.-M., Luminescent Platinum(II) Complexes. Electronic Spectroscopy of Platinum(II) Complexes of 2,2′:6′,2″-terpyridine (terpy) and p-substituted Phenylterpyridines and Crystal Structure of [Pt(terpy)Cl][CF_3SO_3]. *Dalton Trans.* **1993,** 19, 2933-2938.
80. Arena, G.; Calogero, G.; Campagna, S.; Monsù Scolaro, L.; Ricevuto, V.; Romeo, R. Synthesis, Characterization, Absorption Spectra, and Luminescence Properties of Organometallic Platinum(II) Terpyridine Complexes. *Inorg. Chem.* **1998,** *37*(11), 2763-2769.
81. Michalec, J. F.; Bejune, S. A.; Cuttell, D. G.; Summerton, G. C.; Gertenbach, J. A.; Field, J. S.; Haines, R. J.; McMillin, D. R. Long-lived Emissions from 4‘-substituted Pt(trpy)Cl^+ Complexes Bearing Aryl Groups. Influence of Orbital Parentage. *Inorg. Chem.* **2001,** *40*(9), 2193-2200.
82. Barpaga, D.; Nguyen, V. T.; Medasani, B. K.; Chatterjee, S.; McGrail, B. P.; Motkuri, R. K.; Dang, L. X. Insight into Fluorocarbon Adsorption in Metal-organic Frameworks via Experiments and Molecular Simulations. *Sci. Rep.* **2019,** *9*(1), 1-10.
83. Sabale, S.; Barpaga, D.; Yao, J.; Kovarik, L.; Zhu, Z.; Chatterjee, S.; McGrail, B. P.; Motkuri, R. K.; Yu, X.-Y. Understanding Time Dependence on Zinc Metal–Organic Framework Growth Using in Situ Liquid Secondary Ion Mass Spectrometry. *ACS Appl. Mater. Inter.* **2019,** *12*(4), 5090-5098.
84. Thallapally, P. K.; Tian, J.; Radha Kishan, M.; Fernandez, C. A.; Dalgarno, S. J.; McGrail, P. B.; Warren, J. E.; Atwood, J. L. Flexible (Breathing) Interpenetrated Metal−Organic Frameworks for CO_2 Separation Applications. *J. Am. Chem. Soc.* **2008,** *130*(50), 16842-16843.
85. Miskowski, V. M.; Houlding, V. H. Electronic Spectra and Photophysics of Platinum(II) Complexes with Alpha-diimine Ligands. Solid-state Effects. 1. Monomers and Ligand pi Dimers. *Inorg. Chem.* **1989,** *28*(8), 1529-1533.
86. Yersin, H.; Gallhuber, E. On the Lowest Excited States of [Ru$(bpy)_3$]$(PF_6)_2$ Single Crystals. *J. Am. Chem. Soc.* **1984,** *106*(22), 6582-6586.
87. Nozaki, K.; Takamori, K.; Nakatsugawa, Y.; Ohno, T. Theoretical Studies of Phosphorescence Spectra of Tris(2, 2 ‘-bipyridine) Transition Metal Compounds. *Inorg. Chem* **2006,** *45*(16), 6161-6178.
88. Patterson, A. The Scherrer Formula for X-ray particle Size Determination. *Phys. Rev.* **1939,** *56*(10), 978.
89. Moore, R. C.; Pearce, C. I.; Morad, J. W.; Chatterjee, S.; Levitskaia, T. G.; Asmussen, R. M.; Lawter, A. R.; Neeway, J. J.; Qafoku, N. P.; Rigali, M. J. Iodine Immobilization by Materials through Sorption and Redox-driven Processes: A Literature Review. *Sci. Total Environ.* **2020,** *716*, 132820.
90. Levitskaia, T. G.; Chatterjee, S.; Arey, B.W.; Campbell, E. L.; Hong, Y.; Kovarik, L.; Romero, J.; Shutthanandan, V.; Schwenzer, B.; Varga, T. RedOx-Controlled Sorption of Iodine Anions by Hydrotalcite Composites," *RSC Adv.*, **2016**, *6*(79), 76042-76055.